Available online at www.sciencedirect.com
ScienceDirect
International Journal of Thermal Sciences 48 (2009) 781–794
International Journal of Thermal Sciences
www.elsevier.com/locate/ijts

Heat transfer in a mechanical face seal

Noël Brunetière *, Benoit Modolo

Université de Poitiers, UMR CNRS 6610, Laboratoire de Mécanique des Solides, S.P.2M.I., BP 30179, 86962 Futuroscope Chasseneuil Cedex, France

Received 28 August 2007; received in revised form 18 March 2008; accepted 17 May 2008

Available online 20 June 2008

Abstract

This paper presents a numerical analysis of heat transfer in an experimental inner pressurized mechanical face seal, using CFD. The configuration is similar to the laminar flow between a static and a rotating disc bounded by a co-rotating sidewall. A series of simulations allow the authors to propose a correlation for the global Nusselt number for the rotating ring and the static disc. The Nusselt number is a function of the Reynolds number of the flow and the Prandtl number, as well as of the ratio of the fluid and material thermal conductivities. This last conclusion arises from the fact that the heat source is located in the contact between the rotor and the stator and depends on the temperature distribution in the solids. The cooling oil flow appears not to affect the Nusselt number. The numerical results were validated by comparison with measurements carried out on the experimental seal by means of an infrared camera.

Keywords: Convective heat transfer; Infrared thermography; Rotor–stator; Mechanical Face Seal; CFD (Computational Fluid Dynamic)

1. Introduction

Mechanical face seals are used to seal pressurized fluids in rotating machines such as pumps, compressors and agitators, where pressure, temperature and velocity conditions prevent the use of elastomeric seals. These seals are basically composed of a rotating part mounted on to the shaft and a stationary part fixed to the housing. The two parts are maintained in contact by the action of springs and of the pressurized fluid (Fig. 1). Good operating conditions are achieved when the seal faces are partially separated by a thin lubricating fluid film (a fraction of micrometer), avoiding wear on the faces while limiting leakage rate to an acceptable value.

According to Lebeck [1], the behaviour and performance of a mechanical face seal are influenced as much by the thermal behaviour of the seal as by any other factor. Indeed, the dissipated power due to viscous friction and asperities contacts in the sealing interface leads to a significant increase in temperature in the fluid film and in the contiguous solids [2,3]. Consequently, the lubrication conditions are modified because of fluid viscosity variation, thermal distortions of the seal rings and possible phase change. A possible effect of these variations is a drastic increase in leakage rate or seal failure. This is why there have been many studies dealing with thermal effects in recent decades. A brief review is presented in [4]. The main

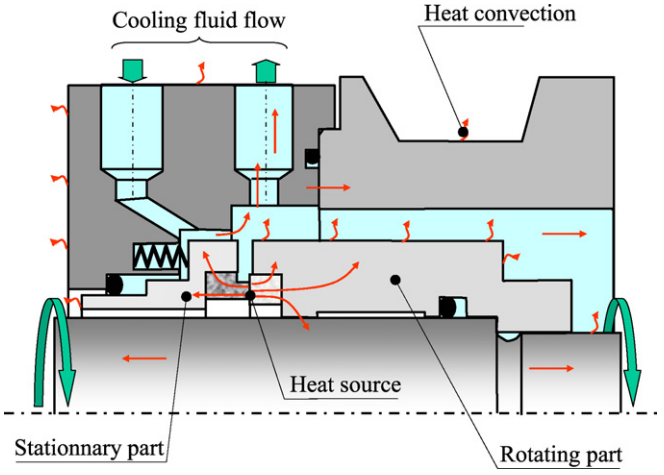

Fig. 1. Example of mechanical face seal.

* Corresponding author.
E-mail address: noel.brunetiere@lms.univ-poitiers.fr (N. Brunetière).

1290-0729/$ – see front matter
doi:10.1016/j.ijthermalsci.2008.05.014

Nomenclature

Cp	fluid specific heat	$\mathrm{J\,kg^{-1}\,°C^{-1}}$
$C_w = \frac{\dot{m}}{\mu R}$	dimensionless mass flow rate (cooling flow)	
$C_{wc} = \frac{\dot{m}_c}{\mu R}$	dimensionless mass flow rate (centrifugally induced flow)	
$G = \frac{H}{R}$	gap ratio	
H	axial clearance	m
k	fluid thermal conductivity	$\mathrm{W\,m^{-1}\,°C^{-1}}$
k_r, k_s	rotor and stator thermal conductivity	$\mathrm{W\,m^{-1}\,°C^{-1}}$
$\dot{m}$	mass flow rate of the cooling flow	$\mathrm{kg\,s^{-1}}$
$\dot{m}_c$	mass flow rate induced by the centrifugal effect	$\mathrm{kg\ s^{-1}}$
$Nu = \frac{qr}{\Delta T k}$	local Nusselt number	
$Nu_{av} = \frac{q_{av} R}{\Delta T_{av} k}$	global Nusselt number	
q	parietal heat flux	$\mathrm{W\,m^{-2}}$
P	dissipated power in the sealing dam	W
$Pr = \frac{\mu Cp}{k}$	Prandtl number	
r	radial coordinate	m
R	inner radius of the rotating ring	m
$Re = \frac{\rho\omega R^2}{\mu}$	Reynolds number	
$Re_r = \frac{\rho\omega r^2}{\mu}$	local Reynolds number	
R_i	inner radius of the stationary disk	m
R_o	outer radius of the rotating ring	m
T	temperature	°C
T_{inlet}	temperature of the oil entering the seal chamber	°C
$U = \frac{u}{\omega r}$, $V = \frac{v}{\omega r}$	dimensionless radial and circumferential fluid velocity	
z	axial coordinate	m

Greek symbols

δ_m, δ_t	thickness of the momentum and thermal boundary layers	m
$\Delta T = T - T_{inlet}$	temperature increase from the inlet fluid temperature	°C
μ	fluid viscosity	Pa s
ρ	fluid density	$\mathrm{kg\,m^{-3}}$
ω	angular velocity	$\mathrm{rad\,s^{-1}}$

Subscripts

av	area weighted average
r	rotor
s	stator

objective of these papers was to measure or determine by a theoretical approach the temperature of the seal faces.

In his book, Lebeck [1] made a comprehensive description of heat transfer in mechanical face seals, presented here in Fig. 1. The heat transfer mechanisms are quite complicated since the seal is surrounded by a complex environment. Because of this feature of the environment, the heat transfer paths are multiple, leading to heat flow computation complications. Nevertheless, the major part of the heat generated in the seal is generally transferred by convection to the sealed fluid in the neighbourhood of the contact. This assumption was confirmed by the simplified analysis of Buck [5] and the numerical study of Brunetiere et al. [6]. This showed that, for a typical configuration, the thermally influenced zone has a length of approximately twice the contact width (i.e. the difference in contact radii) on either side of the sealing interface. Convection around the seal rings is thus of importance in the thermal behaviour of the seal.

At the beginning of the 90's, several authors suggested employing an empirical correlation of the Nusselt number obtained in configurations as similar as possible to mechanical faces seals. Nau [7] considered that the flow in the seal chamber is a Couette Taylor flow. He proposed the use of the formulas obtained by Tachibana et al. [8] and Gazley [9] in the study of heat transfer in an annulus between an inner rotating cylinder and an outer stationary one. A complete review of heat transfer in this type of flow can be found in [10]. On the other hand, Lebeck [1] suggested that the more useful correlation was that of Becker [11], deriving from experiments on a small diameter cylinder rotating in a tank of water. But the range of validity of Becker's formula is too small when compared to Reynolds numbers observed during mechanical face seal operation [1]. Moreover, a mechanical face seal also comprises a static ring for which previous correlations seem to be inapplicable. In 1991, Doane et al. [12] were probably the first authors to carry out Nusselt number measurements on a mechanical face seal. They presented results for the stationary part of the seal, showing a great dependence on the Reynolds number. A few years later, Phillips et al. [13] made similar experiments on the static ring of a mechanical seal. The measured Nusselt numbers exhibited trends close to those obtained with the Gazley [9] and Becker [11] correlations, thus validating the suggestions of Nau [7] and Lebeck [1]. Two years later the same authors [14] presented numerical simulations of heat transfer and fluid flow around their experimental device. This approach, showing good agreement with the experiments, allowed the authors to obtain more information on the local Nusselt number profile along the wetted surfaces. At the same time, Lebeck, Nygren, Shirazi and Soulisa presented both experimental [15] and numerical results [16] relating to heat transfer in a mechanical seal and its surrounding chamber. They emphasized the good agreement between the Nusselt number on the rotating ring and Becker's formula [11]. All the quoted studies deal with turbulent flow. When the sealed fluid is a high viscosity mineral oil, the flow in the seal chamber can be laminar, as was shown by Luan and Khonsari [17]. In their numerical study, Luan and Khonsari only analyze the fluid flow and, more particularly, the interaction between the axial cooling flow and the circumferential Taylor Couette flow induced by the angular motion of the seal.

In all the studies dealing with heat transfer around a mechanical face seal, no author set out to develop a Nusselt number correlation. Moreover, the authors were comparing their findings with empirical formulas obtained in flow involving a uniformly heated rotating cylinder. There is a significant difference here from mechanical face seals, where the heat source is located in the sealing interface. Thus the Nusselt number also depends on the temperature distribution in the seal rings, this being a function of the material properties. In addition, no studies were carried out on inner-pressurized mechanical face seals, a less widespread technology where the sealed fluid is located between the rotating shaft and the seal rings. The aim of the present work is to analyze numerically and, to a lesser extent, experimentally a mechanical face seal. This experimental seal was essentially designed to validate numerical models of the contact behaviour through infrared temperature measurements [3,4] and is thus quite different from industrial mechanical face seals. More particularly, the seal is inner-pressurized and operates with a highly viscous mineral oil resulting in laminar flow. Moreover, the shaft does not pass trough the seal chamber leading to a rotor-stator like flow that is also of interest [18]. Numerical simulations allow the authors to propose a correlation for the Nusselt numbers on the rotating and stationary parts of the seal that are function of the Reynolds number of the flow, the Prandtl number, the ratio of the fluid and the material thermal conductivity. The influence of geometrical parameters has not been analyzed. The numerical and experimental temperature distribution and Nusselt number are in reasonable agreement.

2. Geometrical and operating configuration

2.1. Experimental device

The experimental mechanical face seal is presented in Fig. 2. The carbon rotor is fixed on the shaft by means of a support and a cone expander. The stator, made of a fluorspar disc (CaF_2), is fixed on an annular piston which ensures three degrees of freedom with respect to the frame. This enables a dynamic tracking of any rotor misalignment. The stator is pressed against the rotor by pressurized air acting on the top surface of the annular piston. The thermal properties of the materials of the seal components are given in Table 1. Hydraulic equipment provides oil at controlled pressure and temperature. The oil is a mineral ISO VG 46. Its characteristics are presented in Table 2. The typical operating conditions and the main dimensions of the mechanical face seal are detailed in Table 3.

2.2. Physical background

The oil flow in the mechanical face seal is similar to the flow between a static and a rotating disk with a co-rotating shroud. Owen and Rogers [18] suggested employing the following Reynolds number to characterize the flow regime:

$$Re = \frac{\rho \omega R^2}{\mu} \tag{1}$$

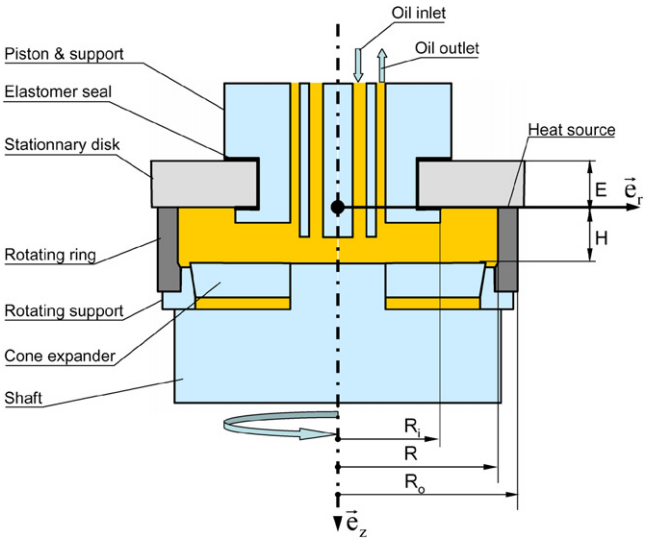

Fig. 2. Experimental device.

Table 1
Material thermal characteristics and assignment

	Thermal conductivity k (W/m °C)	Element
Carbon	15	Rotor
Stainless steel	46	Shaft, piston, supports, expander
Calcium fluoride	9.7	Stator
Elastomer	0.4	seals

Table 2
Fluid properties

Density ρ (kg/m^3)	850
Specific heat Cp (J/kg °C)	2000
Thermal conductivity k (W/m °C)	0.14
Dynamic viscosity μ (Pa s)	0.055 at 35°C

Table 3
Operating conditions and principal dimensions

Angular velocity ω (rpm)	300–1500
Fluid pressure (Pa)	50 000
Inlet fluid temperature (°C)	35
Mass flow rate $\dot{m}$ (kg/s)	0.003–0.015
Inner radius of the rotor R (m)	0.0345
Outer radius of the rotor R_o (m)	0.0385
Inner radius of the disk R_i (m)	0.022
Axial clearance H (m)	0.0122
Disk thickness E (m)	0.01

There is a superposed flow due to the oil circulation whose mass flow rate is $\dot{m}$. We can introduce the non-dimensional flow rate proposed by Owen and Rogers:

$$C_w = \frac{\dot{m}}{\mu R} \tag{2}$$

The flow is also a function of a geometric parameter, this being the gap ratio:

Table 4
Range variation of the dimensionless numbers

Reynolds number Re	600–8000
Dimensionless mass flow C_w	1.5–80
Gap ration G	0.353
Prandtl number	330–1330
Rotor conductivity ratio k/k_r	0.0047–0.037
Stator conductivity ratio k/k_s	0.0072–0.057

$$G = \frac{H}{R} \tag{3}$$

In the simulations presented here, the geometrical configuration remains constant with the axial clearance $H = 12.2$ mm, $R = 34.5$ mm leading to $G = 0.353$ and the Reynolds is varied from about 600 to 8000 (see Table 4). In 1960, Daily and Neece [19] analyzed experimentally an enclosed rotating disc. They observed four different regimes varying with the value of the gap ratio G and the Reynolds number Re. According to their regime chart, the present seal operates in regime II, that is to say a laminar flow with two separated boundary layers, one on each disc

The secondary cooling flow provides a circulation of oil from the rotating part to the stationary part. This is similar to the flow induced by the centrifugal effect. The non-dimensional flow rate is varied from 1.5 to 80.

The heat transfer in the fluid is a function of the flow characteristics and thus depends on the Reynolds number, the flow rate and the gap ratio. However, there is a difference in thermal behaviour and mechanical behaviour that is quantified by the Prandtl number:

$$Pr = \frac{\mu Cp}{k} \tag{4}$$

This number more particularly controls the ratio of the thickness of the momentum boundary layer δ_m to that of the thermal boundary layer δ_t. According to Schlichting [20]:

$$\frac{\delta_m}{\delta_t} = \sqrt{Pr} \tag{5}$$

In the present case the Prandtl number of the oil is varied from 330 to 1330, leading to a ratio value for the thicknesses of the boundary layers of 18 to 36.

In most cases described in the Owen and Rogers book [18], there is an analogy between the mechanical problem and the thermal problem because there is a uniform heat source on the rotating disc that is also obviously a uniform momentum source. In the present case, the heat source is located in the sealing interface. Thus the Nusselt number also depends on the temperature distribution in the seal rings, this being a function of the material properties. It is necessary to introduce another dimensionless parameter:

$$\frac{k}{k_r} \quad \text{or} \quad \frac{k}{k_s} \tag{6}$$

that is, the ratio of the fluid conductivity k to the conductivity of the solid under consideration (k_s for the stator and k_r for the rotor).

The variation range of the dimensionless numbers are given in Table 4.

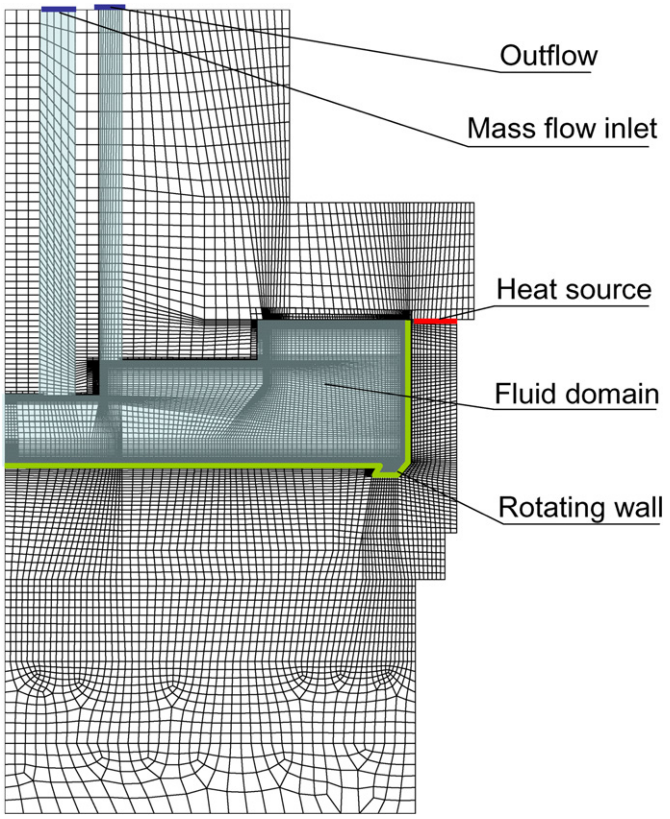

Fig. 3. Numerical model.

3. Numerical model

The simulations were performed by means of the computational fluid dynamic code (CFD) Fluent. The problem is assumed to be axisymmetric. The mesh and the boundary conditions used in the numerical analysis are presented in Fig. 3.

The two-dimensional axisymmetric Navier–Stokes equations, incorporating the circumferential velocity term and continuity equation are solved in the fluid domain. Moreover a tangential momentum equation is also considered for the swirling component of the velocity. As previously said, the fluid flow is laminar. Since the pressure value is not of interest in our study, an inlet mass flow condition is applied at the oil inlet section. It provides a uniform fluid velocity distribution along the inlet section, its magnitude being calculated with respect to the specified mass flow. An outflow condition is used for the outlet section. This condition leads to a zero diffusion flux for all flow variables and ensures an overall mass balance. The zero diffusion flux is physically reached when the flow is fully developed, that is a reasonable assumption when considering the length of the outlet annular pipe (see Fig. 2). Finally, an angular velocity is applied to the rotating walls as indicated in Fig. 3.

The energy equation is solved for the whole domain, including solids and fluid. Because of the high viscosity of the oil, the viscous dissipation is considered in the energy equation. The fluid entering the seal has a uniform temperature of 35 °C. Since it is not possible nor reasonable to solve the lubrication equations in the rotor stator contact, the heat produced in the sealing interface has been modeled by a heat source. To

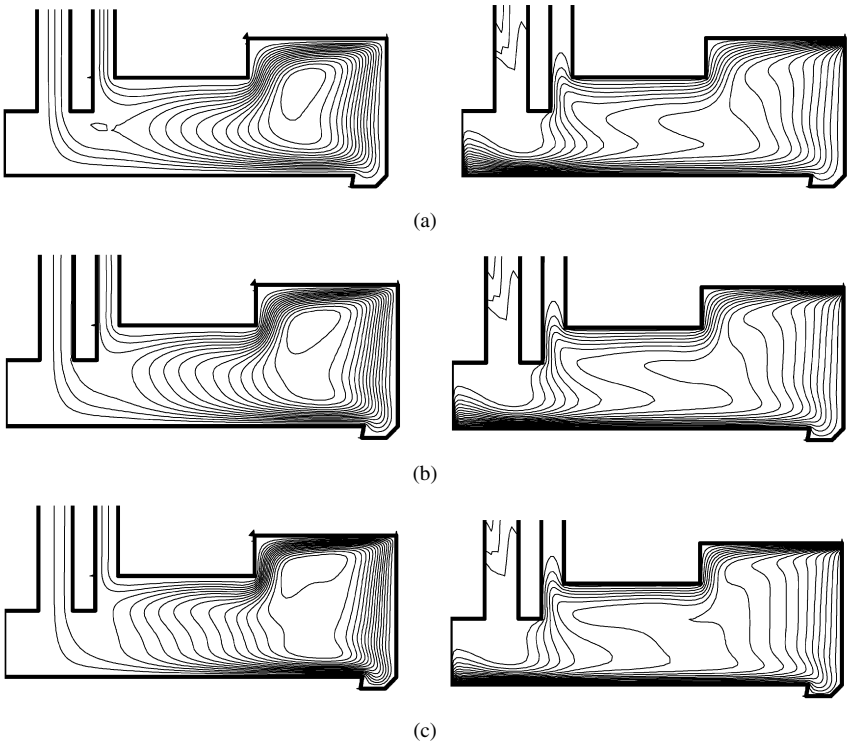

Fig. 4. Streamlines (left) and swirl velocity contour (right) for (a) $Re = 1361$, (b) $Re = 2042$, (c) $Re = 3403$ and $C_w = 10.1$.

this end a thin solid layer has been putted between the rotating ring and the stationary disk as can be seen in Fig. 3, a uniform volumetric heat source being applied in this element. To obtain a reliable heat partition between the solids, the source element is very thin (0.2 mm) and has a high thermal conductivity (1500 $W\,m^{-1}\,°C^{-1}$). The power P introduced in the heat source that is a function of the angular velocity ω is fitted from experimental data in order to simulate realistic cases:

$$P(\omega) = -0.00118\omega^2 + 0.5966\omega - 9.872 \quad \text{with } 60 < \omega < 160\ \text{rad}\,s^{-1} \tag{7}$$

But it is important to note that the value of the dissipated power has no impact on the results presented here because the increase in temperature from the inlet value and the parietal heat fluxes are proportional to the volumetric heat source value.

In this work, the heat transferred to the ambient air has been neglected in order to obtain a simpler numerical model. Indeed, the air flow that is turbulent needs a large amount of nodes to be accurately estimated. However, by using the Becker's correlation [11] to calculate the forced heat convection coefficient around the rotating ring, values ranging from 20 to 35 $W\,m^{-2}\,°C^{-1}$ for the air at 20 °C and atmospheric pressure are found depending on the rotation speed. These values are at least 10 times to 100 times lower than the one calculated for the oil wetted surfaces varying from 380 to about 2000 $W\,m^{-2}\,°C^{-1}$. The natural convection on the upper surface of the disk is assumed to be even lower. Moreover, a previous work showed that the amount of heat transferred to the air is about two orders of magnitude smaller than the amount of heat transported by the oil flow [4]. This assumption is therefore reasonable. In addition, considering the temperature magnitude (lower than 80 °C), the heat transferred by radiation with the environment is neglected. The outer boundaries of the domain are thus adiabatic walls.

As indicated in the previous section, the thermal boundary layer is expected to be very thin because of the great value of the Prandtl number of the oil (see Eq. (5)). Consequently it has been necessary to roughly refine the mesh near the walls as can be seen in Fig. 3. There are at least 6 nodes in the thermal boundary layer for the most severe conditions and about 10 nodes or more in other simulations.

4. Flow analysis

The oil flow in the seal chamber can be compared to the flow between a static disc and rotating disc bounded by a co-rotating sidewall. It was numerically and experimentally studied by Dijkstra and Heijst [21] in 1983, albeit with a gap ratio $G = 0.07$. Lopez [22] carried out a more extensive numerical analysis in 1996 considering a gap ratio of 1.

4.1. Effect of Re

Fig. 4 shows the streamlines and the dimensionless swirl velocity contour for three different values of Reynolds number. The swirl velocity is defined in this way:

$$V = \frac{v}{\omega r} \tag{8}$$

As can be seen on the streamline plots, oil recirculation from the rotating part to the stationary part appears due to the centrifugal effect. The centre of the cell is located near the contact area (i.e. the upper edge of the rotating ring) as shown by Lopez. An

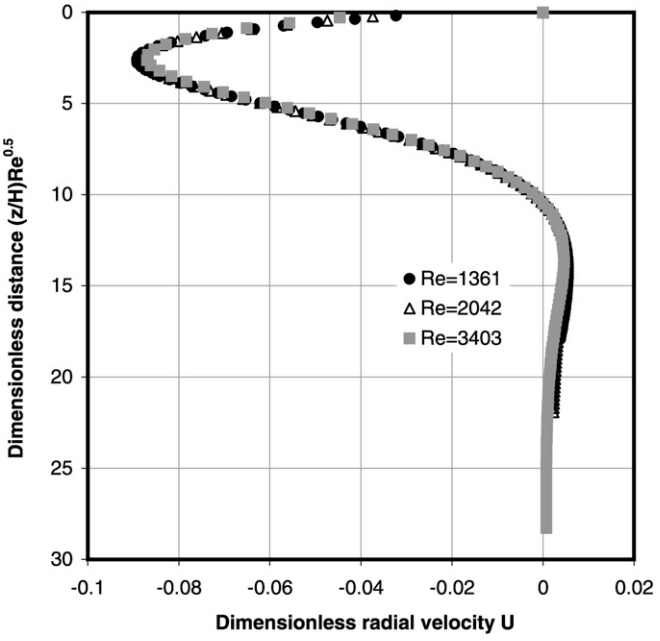

Fig. 5. Dimensionless radial velocity versus the dimensionless distance from the upper wall at $r/R = 0.81$ and $C_w = 10.1$.

increase in the Reynolds number leads to a displacement of the cell in the direction of the static disc and to the development of a secondary cell in the vicinity of the lower wall.

In the outer region, where the vertical distance between the walls is higher, two distinct boundary layers can be observed. They are separated by a core region where the fluid exhibits a quite uniform swirl velocity in the axial direction. Moreover, the thickness of the boundary layers is a decreasing function of the Reynolds number. In the inner region where the stationary and rotating walls are closer, no core region develops at all for the Reynolds number considered in the present study.

The dimensionless radial velocity at $r/R = 0.81$ is shown in Fig. 5 as a function of the dimensionless distance from the static disc, the figure referring to the three Reynolds number values considered in the previous graph. The dimensionless radial velocity is:

$$U = \frac{u}{\omega r} \tag{9}$$

Following Lopez, the distance has been re-scaled according to the square root of the Reynolds number, leading to perfect superposition of the velocity profiles. This figure shows that the thickness of the boundary layer is inversely proportional to the square root of the Reynolds number. Since the velocity magnitude is controlled by the angular velocity, the radial flow rate along the stator is only due to the centrifugal effect and not generated by the oil cooling flow. Considering the area of negative velocity in Fig. 5, the value of the mass flow naturally induced by the centrifugal effect can be estimated:

$$\dot{m}_c \approx 0.97\pi H\rho \frac{\omega R^2}{\sqrt{Re}} \tag{10}$$

Similarly as for the cooling flow, it is possible to define a dimensionless mass flow rate:

$$C_{wc} = \frac{\dot{m}_c}{\mu R} = 0.97\pi G\sqrt{Re} \tag{11}$$

4.2. Effect of C_w

Fig. 6 shows the streamlines and the dimensionless swirl velocity contour for three different values of the dimensionless mass flow and $Re = 2042$. It can be seen that, for those values of the dimensionless mass flow considered, only the flow in the inner region, where the stator and rotor are closest, is affected. More particularly, an increase in C_w leads to the development of a recirculation cell in the inner zone. For the higher value of the mass flow rate, a substantial part of the inlet cooling flow is driven to the outlet without flowing through the outer zone and thus does not participate in the cooling of the seal rings. The ratio of the imposed flow rate C_w to the natural flow rate C_{wc}, calculated from Eq. (11), is 1.66 in this case and remains lower than one in the two other cases. It shows that, as a consequence of the centrifugal effect, an imposed flow rate higher than the centrifugally induced flow rate is ineffective in improving oil circulation. Luan and Khonsari arrived at similar conclusions in their study of an outer-pressurized mechanical face seal [17].

No noticeable difference can be observed in the flow in the outer area. Indeed, if the dimensionless radial velocity at $r/R = 0.81$ is presented as a function of the dimensionless distance from the static disc (re-scaled according to the square root of the Reynolds number, as shown in Fig. 7), the imposed mass flow does not modify the superposed velocity profiles. However, it is noted that an increase in C_w can slightly reduce the mass flow rate in the stator boundary layer.

5. Heat transfer analysis

As suggested by Owen and Rogers [18], we are interested by the increase in temperature from the inlet cooling flow temperature. Thus all the results are in given in terms of difference between the local temperature and the inlet oil temperature that is used as a temperature reference. An example of temperature distribution in the oil and the solids is presented in Fig. 8. As anticipated, the temperature is maximal in the contact area between the static disc and the rotating ring, this being a heat source. The temperature in the solids decreases progressively as the distance from the heat source rises. The temperature in the oil appears to be uniform. Only a very thin thermal boundary layer can be observed in the vicinity of the walls. The thickness of the boundary layer is not surprising because, according to Eq. (5), it should about 25 times thinner than the momentum boundary layer.

The temperature profile near the stator at $r/R = 0.81$ is presented in Fig. 9 for different values of Reynolds number. In agreement with Eq. (5), the thermal boundary layer is similar to the momentum boundary layer and can thus be re-scaled by the square root of the Reynolds number. However, if Figs. 5 and 9 are compared, the ratio of the boundary layer thicknesses is found to be 8. This is less than the value 25 calculated from Eq. (5).

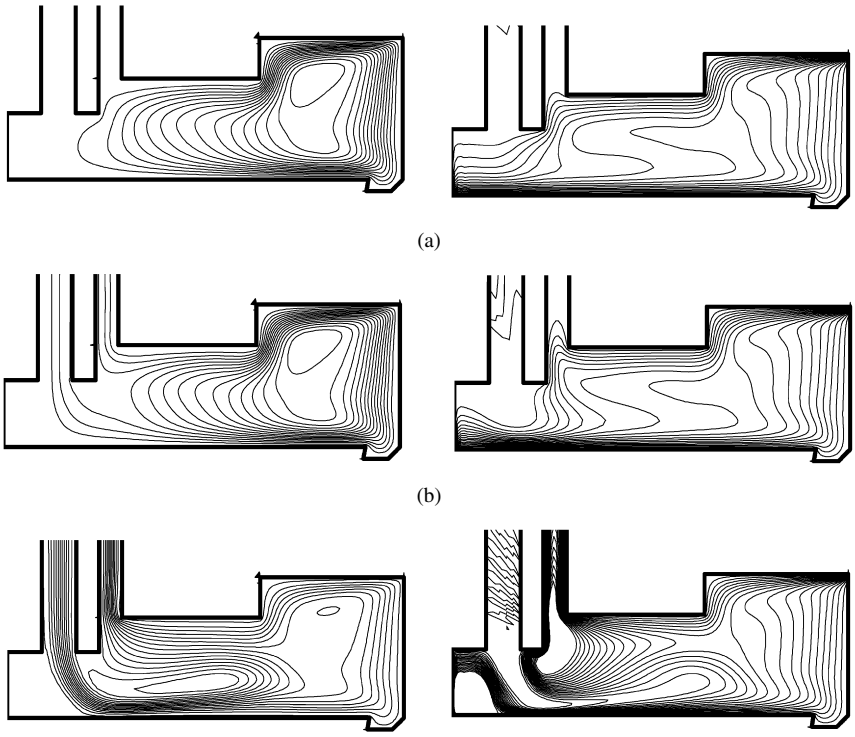

Fig. 6. Streamlines (left) and swirl velocity contour (right) for (a) $C_w = 2.53$, (b) $C_w = 10.1$, (c) $C_w = 80.9$ and $Re = 2042$.

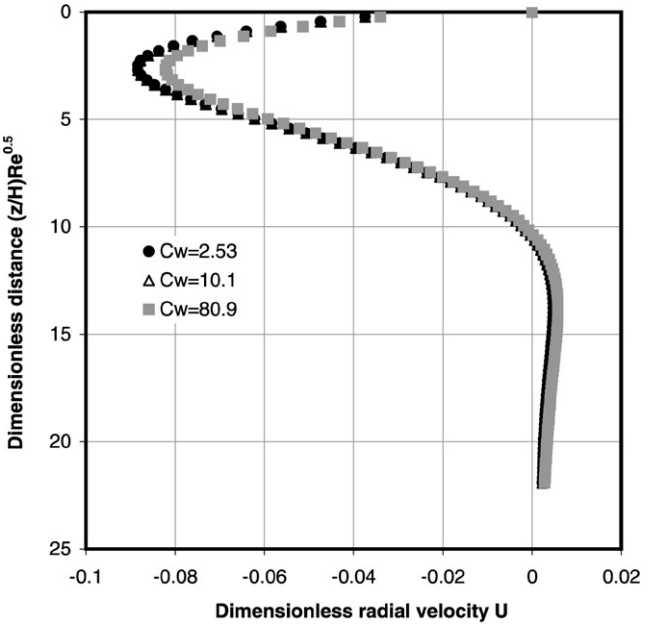

Fig. 7. Dimensionless radial velocity versus the dimensionless distance from the upper wall at $r/R = 0.81$ and $Re = 2042$.

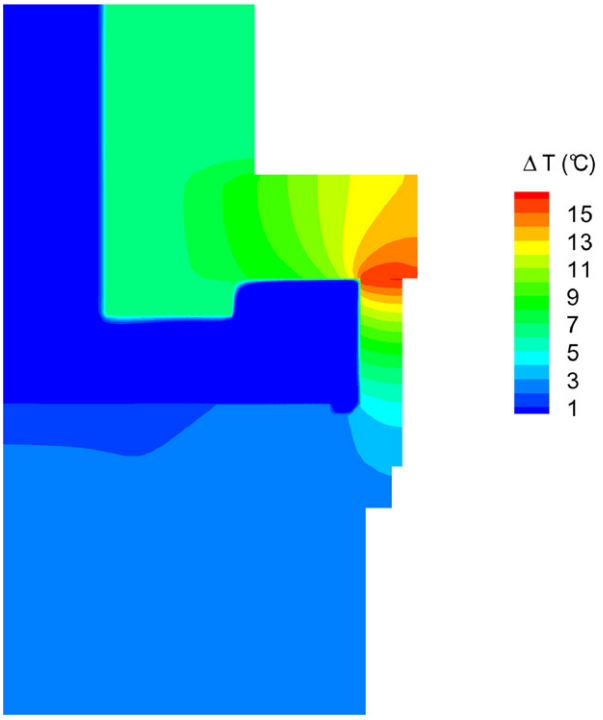

Fig. 8. Temperature distribution in the oil and the solids ($Re = 2042$, $C_w = 10.1$, $Pr = 667$, $k/k_s = 9.7$ and $k/k_r = 15$).

5.1. Local Nusselt number

The distribution of the local Nusselt number along the wetted surface will be first analyzed. The Nusselt number for the rotating ring is:

$$Nu = \frac{qR}{\Delta T k} \tag{12}$$

where q is the parietal heat flux that can be obtained according to the temperature gradient in the rotor:

$$q = k_r \frac{\partial T}{\partial r}(r = R) \tag{13}$$

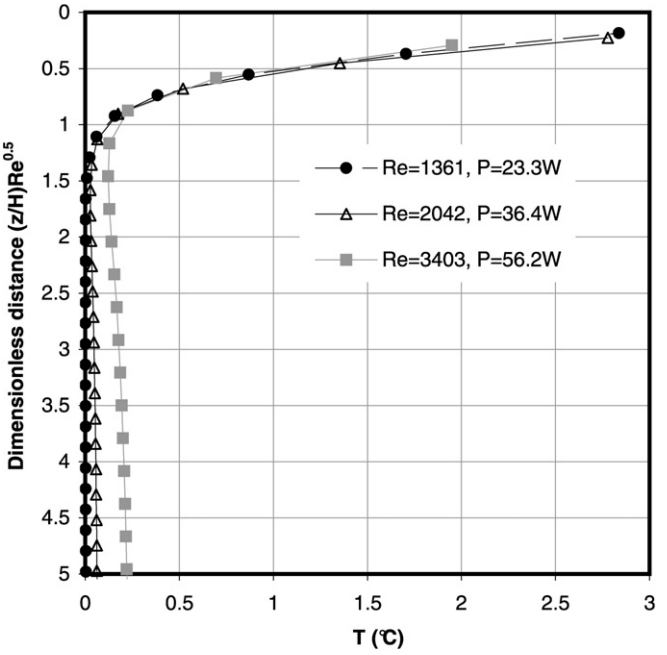

Fig. 9. Temperature increase versus the dimensionless distance from the upper wall at $r/R = 0.81$ and $C_w = 10.1$, $Pr = 667$, $k/k_s = 9.7$ and $k/k_r = 15$.

This term can be easily obtained in the case of CFD simulations. The distribution of the local Nusselt number along the rotating ring is presented in Fig. 10(a) for three different Reynolds number values, the other parameters being unchanged. All the curves presented in Fig. 10(a) have a similar shape. A peak is observed in the bottom of the ring (i.e. close to Z-coordinate 1). This is due to the interaction with the boundary layer generated by the centrifugal force on the rotating disk. After this peak, the local Nusselt increases again, though more gradually. It then rises sharply and decreases abruptly in the vicinity of the contact (i.e. at Z-coordinate 0). The increase in Nusselt number is the result of the increase in surface temperature as the distance from the heat source decreases. The sharp reduction near the edge of the rotor is due to the corner between the surfaces leading to an increase in the distance from the streamlines to the surfaces, as can be seen in Figs. 4 and 6. As expected, an increase in Reynolds number leads to a reduction of the thermal boundary layer and thus to a better cooling of the surface. Since, the thermal boundary layer is inversely proportional to the square root of the Reynolds number, it is convenient to re-scaled the Nusselt number in this way. Moreover, to underline the effect of the interaction with the boundary layers on the stationary upper surface, it is interesting, as suggested by Lopez [22], to multiply the x-axis of Fig. 10(a) by the square-root of the Reynolds number. This is done in Fig. 10(b). This figure shows that the magnitude and the width of the left hand side peak in Nusselt number distribution is controlled by the square root of Re. The same work has been done for the lower wall in Fig. 10(c) and the conclusions are identical.

The Nusselt number for the stationary disk is defined by using the local radius r:

$$Nu = \frac{qr}{\Delta T k} \tag{14}$$

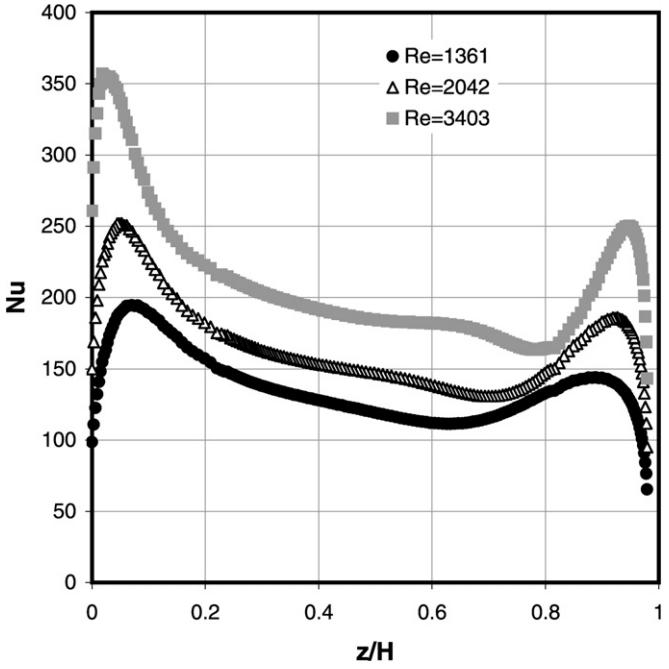

(a)

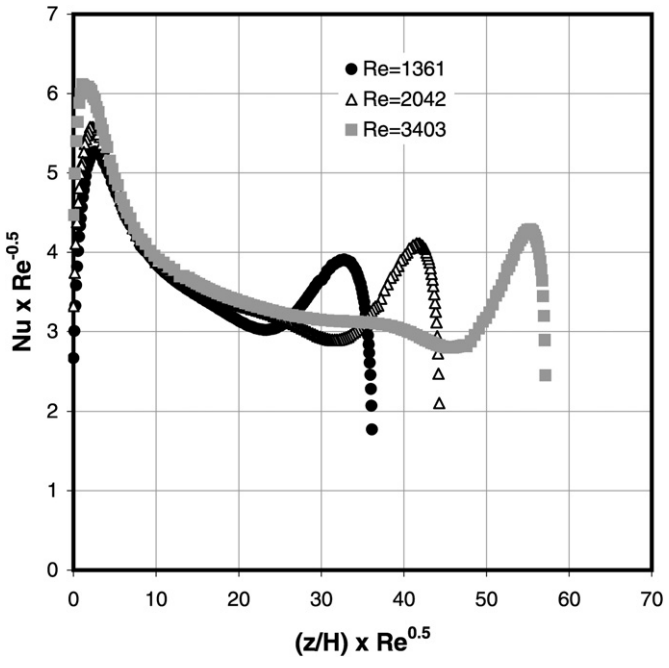

(b)

Fig. 10. Local Nusselt number distribution along the rotating ring obtained with $C_w = 10.1$, $Pr = 667$, $k/k_s = 9.7$ and $k/k_r = 15$: (a) Nusselt number versus the axial coordinate, (b) re-scaled Nusselt number in upper coordinate, (c) re-scaled Nusselt number in lower coordinate.

The parietal flux q can be computed from the temperature distribution in the stator:

$$q = k_s \frac{\partial T}{\partial z}(z = H) \tag{15}$$

The results for the static disc are presented in Fig. 11(a). The three curves also have a similar shape, an increase in Reynolds number providing a more efficient heat transfer. As for the ro-

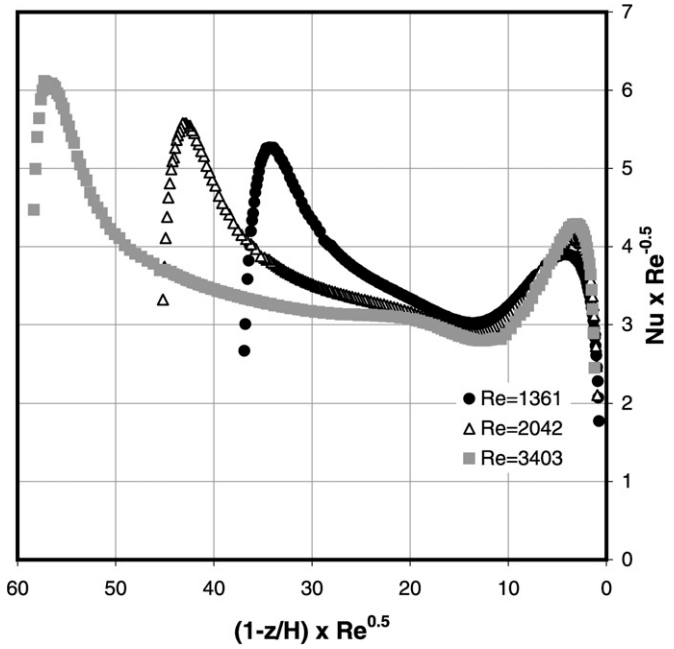

(c)

Fig. 10. (Continued.)

tating ring, the Nusselt number is close to zero in the vicinity of the contact and then increases sharply. After that, the Nusselt number decreases gradually to zero along the disc radius. These changes can be attributed to the decrease in the surface temperature and to the increase in distance from the streamlines to the disc surfaces, as shown in Figs. 4 and 6. The position of the peak observed near the contact can be related to the boundary layer thickness developed on the rotating ring, this being a decreasing function of the Reynolds number. To analyze this effect, the Nusselt number has been re-scaled according to the local Reynolds number Re_r and presented in Fig. 11(b) as a function of a modified coordinate as done for the rotor. The peaks located at the outer radius have a quite close width but a slight difference in magnitude. It is important to note the thickness of the boundary layer developed on the rotating ring is largely greater than those located on the disks, as can be seen on Fig. 4. The interaction with the Nusselt number distribution on the stator is thus not so clear as for the rotor.

Fig. 12 presents the evolution of the Nusselt number on the rotating ring and on the stationary disk for three different values of the dimensionless mass flow C_w. It has been previously shown that this number does not affect the flow in outer region of the seal chamber (Figs. 6 and 7). As a consequence, C_w has an almost insignificant effect on the Nusselt number distributions on the two surfaces.

The thermal parameters that is to say the Prandtl number and the conductivity ratios appear to not modify the shape of the local Nusselt curves but only their magnitude. The Nusselt distributions are thus only controlled by the flow structure and essentially by the Reynolds number. The influence of thermal parameters is not presented in this section but analyzed in the following paragraph.

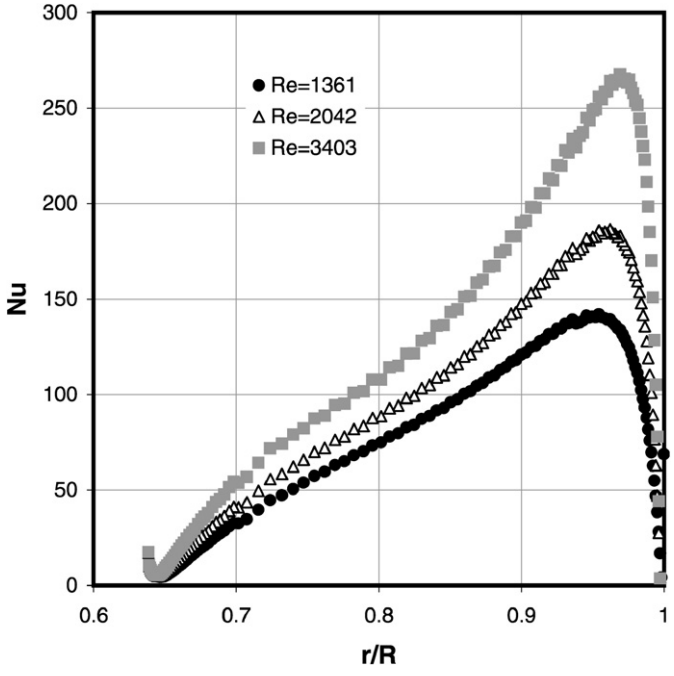

(a)

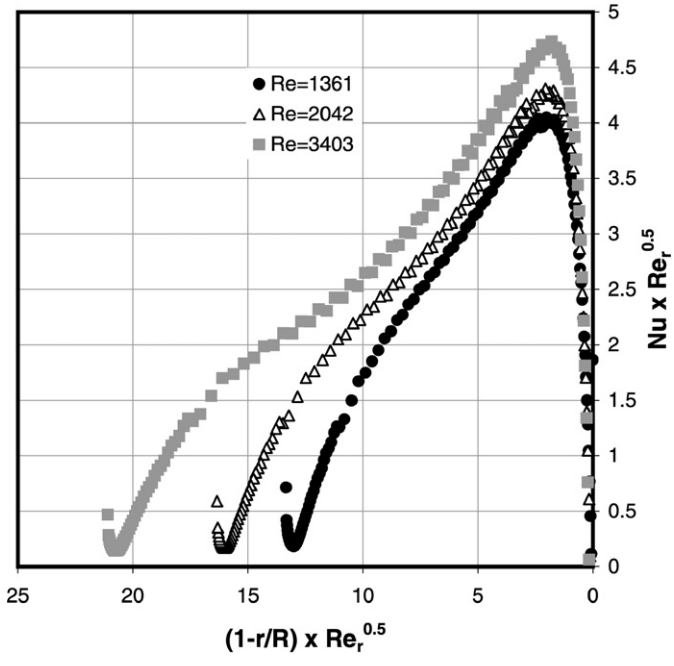

(b)

Fig. 11. Local Nusselt number distribution along the stationary disk obtained with $C_w = 10.1$, $Pr = 667$, $k/k_s = 9.7$ and $k/k_r = 15$: (a) Nusselt number versus the radial coordinate, (b) re-scaled Nusselt number in outer coordinate.

5.2. Global Nusselt number

The heat globally transferred from the seal elements to the oil is evaluated by means of an averaged Nusselt number, that is of interest in mechanical seals. The objective of this section is to propose a correlation between this number and the other dimensionless parameters. It is defined in the way proposed by Owen and Rogers [18]:

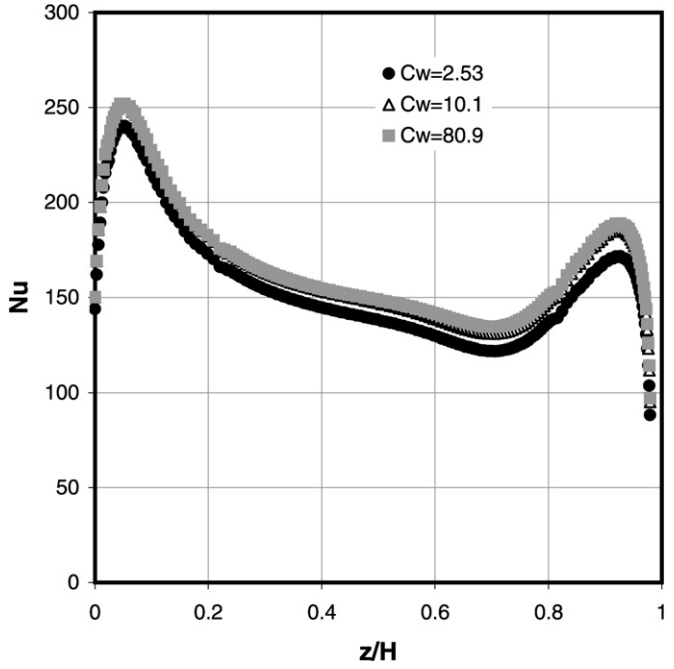

(a)

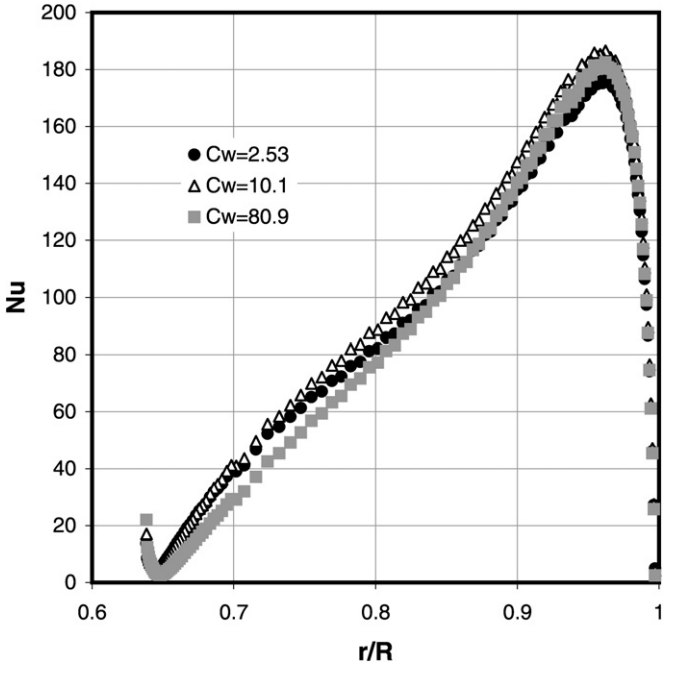

(b)

Fig. 12. Local Nusselt number distribution obtained with $Re = 2042$, $Pr = 667$, $k/k_s = 9.7$ and $k/k_r = 15$: (a) along the rotating ring, (b) along the stationary disk.

$$Nu_{av} = \frac{q_{av} R}{\Delta T_{av} k} \tag{16}$$

where q_{av} is the area-weighted average heat flux and ΔT_{av} is the area-weighted average difference between the local temperature and the inlet oil temperature:

$$q_{av} = \frac{1}{S} \int_s q \, dS$$

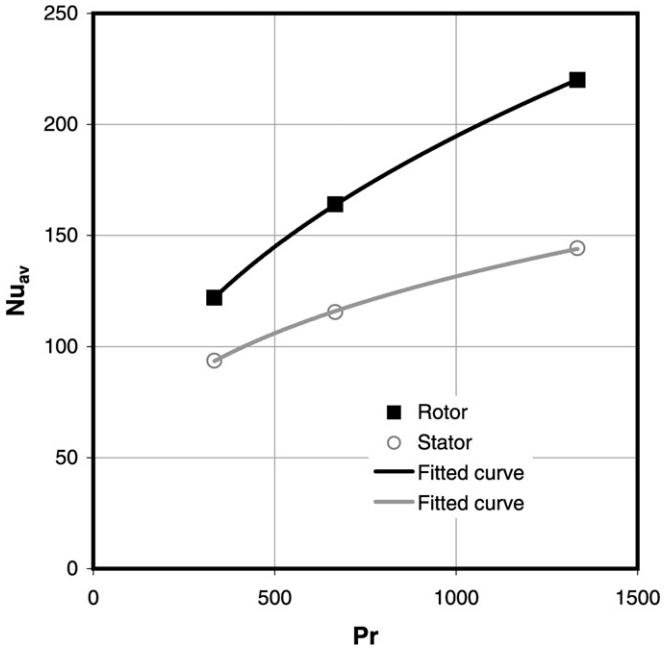

Fig. 13. Global Nusselt number versus the Prandtl number ($Re = 2042$, $C_w = 10.1$, $k/k_s = 9.7$ and $k/k_r = 15$).

$$\Delta T_{av} = \frac{1}{S} \int_s \Delta T \, dS \tag{17}$$

In Eq. (17), S is the surface of interest that is area of the stator or the rotor in contact with oil.

The influence of the Prandtl number on the Nusselt number is presented in Fig. 13. In the first place, it can be seen that heat transfer is more efficient on the rotor where the oil has a lower temperature than when flowing along the stator. As expected, Nu is an increasing function of Pr. On the rotating ring, the Nusselt number curve can be fitted in this way:

$$Nu_{av\,r} \sim Pr^{0.4259} \tag{18}$$

The Nusselt number on the stator is also a power function of the Prandtl number:

$$Nu_{av\,s} \sim Pr^{0.312} \tag{19}$$

The value of the exponent is less than that for the rotor, the Nusselt number thereby exhibiting a reduced dependence on the Prandtl number. The exponent of both power laws is lower than the theoretical value (0.5) given in Eq. (5). This difference is probably due to the fact that the heat source is located in the contact area, with heat transfer depending on the temperature distribution in the solids as well as in the fluid flow. However, if Eq. (19) is used to calculate the ratio of the thickness of the momentum and thermal boundary layers on the stator, a value of 7.6 is found (corresponding to $Pr = 667$). This is in excellent agreement with the ratio of the thicknesses shown in Figs. 5 and 9.

Fig. 14 presents the change in the global Nusselt number on the stator and the rotor as a function of the dimensionless mass flow C_w. As previously shown, it has no effect on heat transfer. However a slight decrease in Nusselt number can be observed for the stator at high values of C_w. This is not surprising as

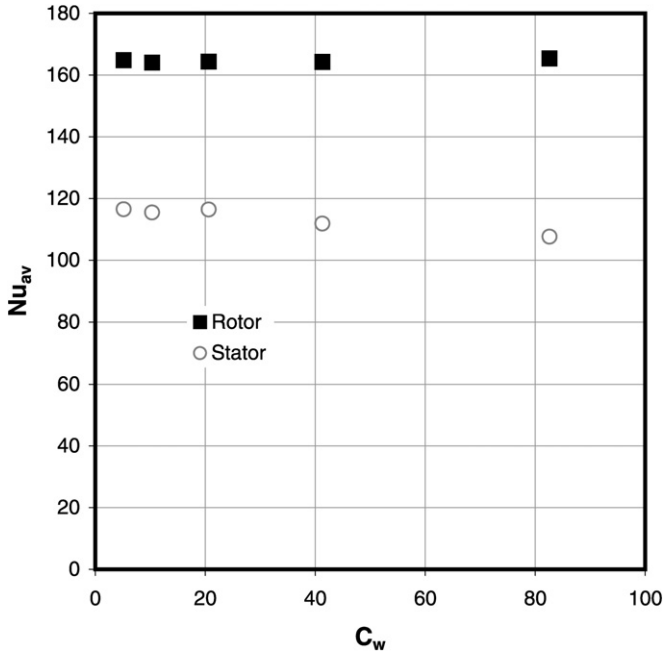

Fig. 14. Global Nusselt number versus the dimensionless mass flow ($Re = 2042$, $Pr = 667$, $k/k_s = 9.7$ and $k/k_r = 15$).

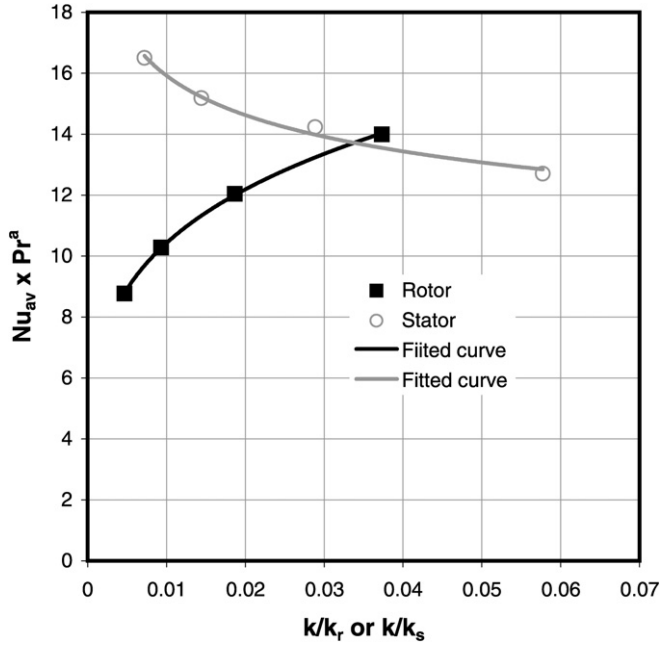

Fig. 15. Nusselt number scaled by the Prandtl number ($a = -0.4259$ for the rotor and $a = -0.312$ for the stator) versus the conductivity ratio ($Re = 2042$, $C_w = 10.1$).

an increase in C_w can lead to a small reduction in the natural cooling flow rate, as is shown in Fig. 7. Thus, the decision is taken to neglect the effect of C_w in the Nusselt correlation.

The influence of the thermal conductivity ratio (Eq. (6)) on the Nusselt number is shown in Fig. 15. To perform this analysis the conductivity of the solids is varied along with the fluid conductivity, thereby leading to a variation in the Prandtl number. To prevent this effect, the Nusselt number was scaled according to the power law (18) for the rotor and (19) for the stator. The

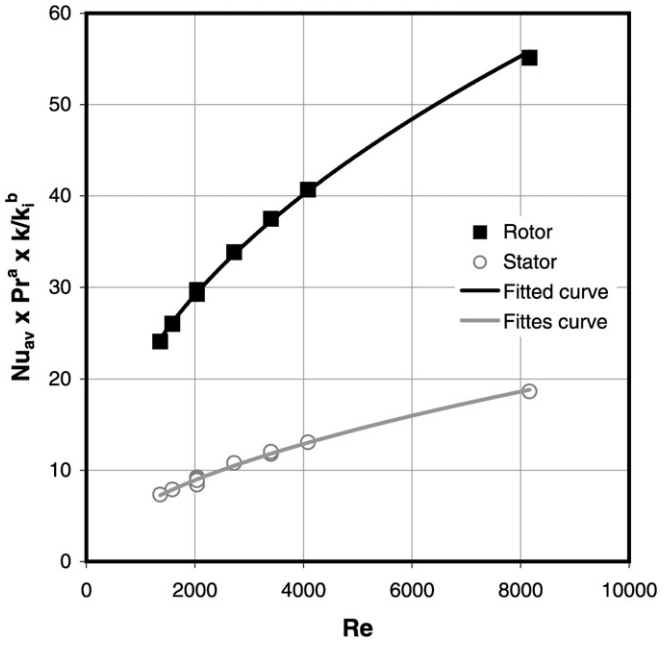

Fig. 16. Nusselt number scaled by the Prandtl number and the conductivity ratio versus the Reynolds number.

resulting graph is interesting because it shows the influence of a parameter that generally has no effect on the Nusselt number. Indeed, in many works [8–11] the solids constitute a uniform heat source, their conductivity having no effect. In the present case, the distribution of heat transferred from the solids to the fluid depends on the conductivity of the solids because of the localized heat source. Another interesting point is the contrasting behaviour of the Nusselt number of the stator and of the rotor: the Nusselt number is an increasing function of the conductivity ratio for the rotor whereas it is a decreasing function in the case of the static wall. This difference can be explained in terms of the oil flowing along the rotor from the coldest point to the hottest point located near the contact, whereas the flow direction runs counter to the temperature distribution along the stator. The Nusselt curves can be fitted in this way:

$$Nu_{\mathrm{avr}} \times Pr^{-0.4259} \sim \left(\frac{k}{k_r}\right)^{0.2251} \tag{20}$$

$$Nu_{\mathrm{avs}} \times Pr^{-0.312} \sim \left(\frac{k}{k_s}\right)^{-0.1225} \tag{21}$$

Finally, the Nusselt numbers on both surfaces are presented as a function of the Reynolds number in Fig. 16. To take account of all simulations performed with various Prandtl numbers and conductivity ratios, the Nusselt number has been scaled using Eqs. (18)–(21). The Nusselt number obviously increases as a function of the Reynolds number. The final correlations for the Nusselt numbers are:

$$Nu_{\mathrm{avr}} = 0.8706 \times Re^{0.4619} Pr^{0.4259} \times \left(\frac{k}{k_r}\right)^{0.2251} \tag{22}$$

$$Nu_{\mathrm{avs}} = 0.157 \times Re^{0.5314} \times Pr^{0.312} \times \left(\frac{k}{k_s}\right)^{-0.1225} \tag{23}$$

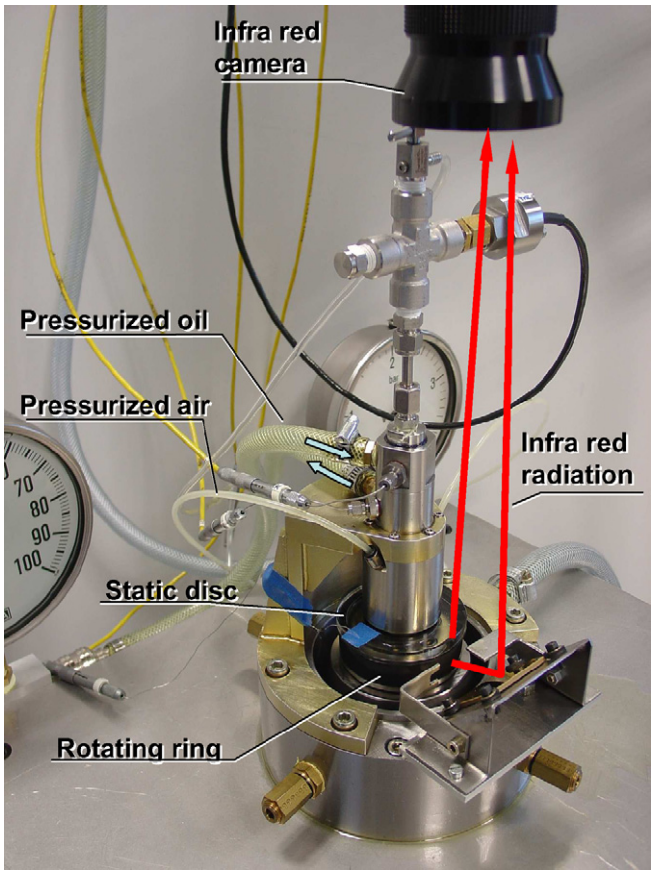

Fig. 17. Experimental set up.

As discussed in the previous section dealing with local Nusselt number, the exponent of the Reynolds number is close to 0.5 for the two Eqs. (22) and (23). This is not surprising because we previously showed that the thermal boundary layer is scaled according to the square root of the Reynolds number (Fig. 9). While studying an experimental unshrouded rotor – stator system operating in a laminar flow regime, Boutarfa and Harmand [23] found that when the gap ratio is higher than 0.02, the Nusselt number on the rotating disk is a function of the square root of the Reynolds number. This is in quite good agreement with the present work.

6. Comparison with experiments

This section deals with the comparison between numerical results and experiments. The experimental set-up is described in Fig. 17. An infra red camera placed above the mechanical face seal allows the temperature distribution to be determined on the face of the rotor through the static fluorspar disc and the lubricating film. Moreover, the temperature on the outer surface of the carbon ring is measured by means of a mirror placed as illustrated in Fig. 17. The radiometric equations that have to be solved in order to obtain the carbon ring temperature are presented in [24]. The presence of two dioptres, as a consequence of the semi-transparent media (oil and fluorspar), leads to a degree of complexity in the radiometric equation for the upper surface temperature.

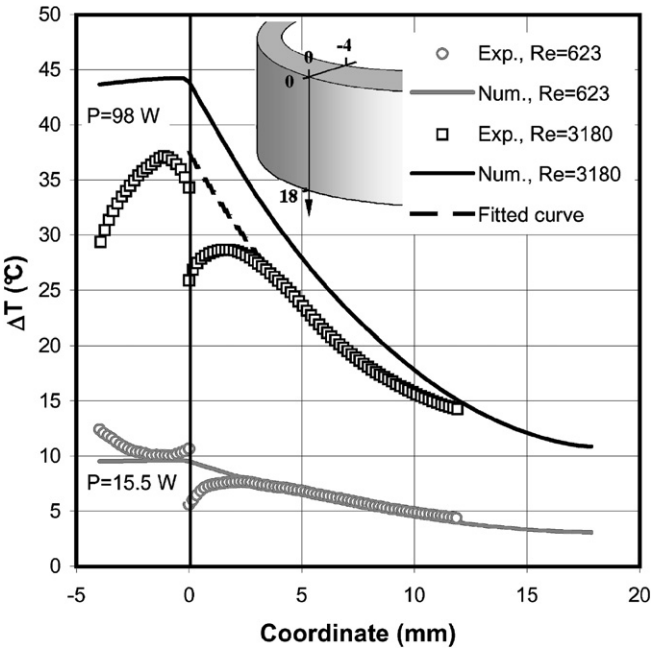

Fig. 18. Comparison of temperature profiles on the rotor ($C_w \approx 1.6$ and $Pr \approx 750$).

The power dissipated in the contact is measured by an electric technique. The power consumed by the electrical motor driving the shaft is measured without the seal. The power dissipated in the contact is thus given by the difference between the electrical power consumed with and without the seal. This method regrettably exhibits a level of uncertainty that can be in excess of 10%. In terms of temperature measurements, this uncertainty represents about 2 °C.

Because of the experimental technique, the comparison between numerical results and measurements can only be carried out on the rotating ring.

6.1. Comparison of temperature profiles on the rotor

Fig. 18 presents temperature distributions along the rotor obtained numerically and experimentally. The top surface of the rotor is described by negative values of the co-ordinate, whereas positive values correspond to points located on the outer surface of the ring as shown in Fig. 18. The maximal values of the temperature predictably occur on the contacting face. The temperature on the surrounding surface decreases progressively from the contact temperature to a smaller value at the end surface of the ring. It can be seen that experimental distributions on the outer surface of the rotor decrease when approaching the contact surface in the few millimetres near this surface. There is consequently a temperature discontinuity at the edge of the ring, indicating a measurement discrepancy. This problem is due to oil leakage leading to the formation of an oil meniscus between the upper part of the rotor and the end radius of the static disc. This is the source of the temperature underestimation.

In order to make comparisons, the measured dissipated power has been introduced in the numerical model before computing temperatures (values are given in Fig. 18). For the lower

value of the Reynolds number, a good agreement between numerical and experimental results is observed. In the second case, the simulation provides a temperature distribution higher than the measured one. This difference can be explained by the degree of uncertainty in the measurement of dissipated power.

Another curve has been added to the graph. Indeed, we observed that if the erroneous points are eliminated, the experimental temperature profiles on the outer surface can be accurately fitted using a second order polynomial function, as shown in Fig. 18.

6.2. Comparison of Nusselt numbers on the rotor

To estimate the global Nusselt number on the rotor, it is necessary to perform several calculations in order to obtain the heat flux and the temperature at the inner radius of the ring. To this end, the conductivity equation in the rotor has to be solved:

$$\frac{1}{r}\frac{\partial T}{\partial r}+\frac{\partial^2 T}{\partial r^2}+\frac{\partial^2 T}{\partial z^2}=0 \tag{24}$$

The outer surface of the ring is assumed to be adiabatic:

$$\frac{\partial T}{\partial r}=0 \quad \text{at } r=R_\mathrm{o} \tag{25}$$

Moreover, we previously indicated that the temperature on the outer surface could be accurately fitted using a polynomial function of the second order:

$$T(z)=a\times z^2+b\times z+c \quad \text{at } r=R_\mathrm{o} \tag{26}$$

A particular solution of this set of equations is:

$$T(r,z)=aR_\mathrm{o}^2\left[\ln\left(\frac{r}{R_\mathrm{o}}\right)+0.5\left(1-\frac{r^2}{R_\mathrm{o}^2}\right)\right]+az^2+bz+c \tag{27}$$

The average parietal heat flux at the inner radius of the rotor is:

$$q_\mathrm{av}=\frac{1}{H}\int_0^H k_\mathrm{r}\frac{\partial T}{\partial r}(R,z)\,\mathrm{d}z=k_\mathrm{r}aR_\mathrm{o}^2\left(\frac{1}{R}-\frac{R}{R_\mathrm{o}^2}\right) \tag{28}$$

The average temperature is:

$$\begin{aligned}T_\mathrm{av}&=\frac{1}{H}\int_0^H T(R,z)\,\mathrm{d}z\\&=aR_\mathrm{o}^2\left[\ln\left(\frac{R}{R_\mathrm{o}}\right)+0.5\left(1-\frac{R^2}{R_\mathrm{o}^2}\right)\right]+\frac{aH^2}{3}+\frac{bH}{2}+c\end{aligned} \tag{29}$$

Thus, knowing the coefficients of the fitted curve (26) and the oil inlet temperature, we can easily obtain the global Nusselt number (Eq. (16)) from the average heat flux (28) and temperature (29). The experimental values of the Nusselt number at different values of the dimensionless flow rate are presented in Fig. 19 as a function of the Reynolds number. Because of inlet oil temperature accompanied by viscosity variation from one test to the other, the effect of the Prandtl number was nullified using Eq. (18). The experimental results are compared to the numerical correlation given in Eq. (22). A reasonable agreement between simulations and experiments is achieved, the average difference being close to about 15% of the theoretical value. The comparison shows that the dimensionless flow rate has only a small effect on the Nusselt number when compared to the Reynolds number influence. The dependence of the heat transfer on the Reynolds number is experimentally validated.

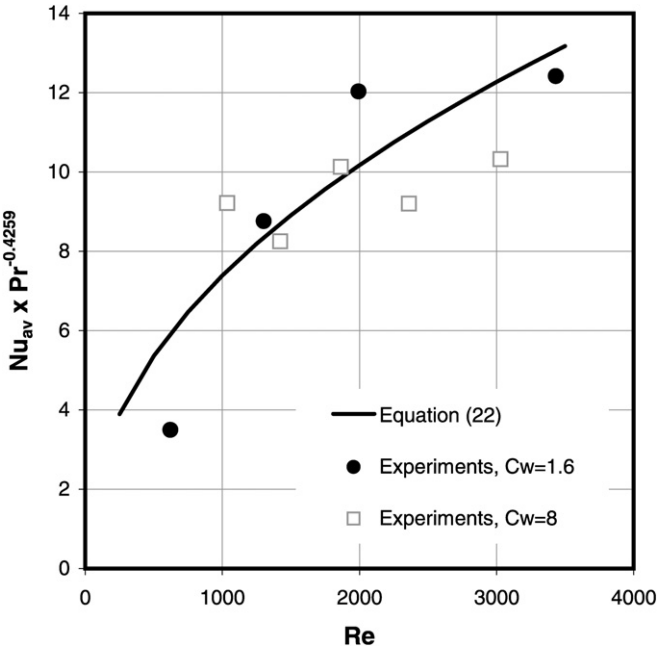

Fig. 19. Comparison of Nusselt numbers on the rotor.

7. Conclusion

The temperature of the faces is a key parameter in a mechanical seal. Its value is greatly dependent on heat transfer with the surrounding sealed fluid, this being able to be characterized by a Nusselt number. No correlations can be found in the literature. To this end, a numerical study based on CFD was developed on an inner-pressurized mechanical face seal. The sealed fluid is a highly viscous mineral oil resulting in a laminar flow regime. The configuration is similar to the flow between a static disc and rotating disc bounded by a co-rotating sidewall. The momentum boundary layer thickness is inversely proportional to the square root of the Reynolds number. It has been shown that a cooling flow rate higher than the one naturally induced by the centrifugal effect is not favourable, part of the oil being driven directly to the outlet.

A number of simulations allow us to propose a correlation for the global Nusselt number on the rotating ring and the static disc. The Nusselt number is approximately proportional to the square root of the Reynolds number, but exhibits a lower dependence on the Prandtl number. The cooling flow has only a weak effect on heat transfer. Moreover, because the heat source is located in the contact, the Nusselt number is also a func-

tion of the ratio of the fluid and material thermal conductivities. The relation (an increasing or decreasing function) depends on the direction of the flow and the temperature distribution in the solids. A higher conductivity is favourable if the oil flows from the hottest to the coldest points of the solids and unfavourable if vice versa. This is an interesting conclusion since mechanical face seals are generally composed of a ring made from a material such as silicon carbide, an excellent thermal conductor, plus a carbon ring whose thermal conductivity is about ten times lower. The result of the current work would suggest orienting the flow from the carbon to the silicon carbide ring. As previously observed in mechanical face seals, the local Nusselt number can vary significantly along the seal elements.

The theoretical correlation was validated through a comparison with experimental findings. The temperature distribution on the experimental cell was determined by infrared thermography and reasonable agreement was obtained for the temperature profiles.

References

[1] A.O. Lebeck, Principles and Design of Mechanical Face Seals, Wiley-Interscience Publication, John Wiley and Sons, New York, 1991.
[2] F.K. Orcutt, An investigation of the operation and failure of mechanical face seals, Journal of Lubrication Technology 91 (1969) 713–725.
[3] B. Tournerie, D. Reungoat, J. Frêne, Temperature measurements by infrared thermography in the interface of a radial face seal, Journal of Tribology 113 (1991) 571–576.
[4] N. Brunetière, B. Tournerie, J. Frêne, TEHD lubrication of mechanical face seals in stable tracking mode. Part 1: Numerical model and experiments, Journal of Tribology 125 (2003) 608–616.
[5] G.S. Buck, Heat transfer in mechanical seals, in: Proceedings of the 6th Pump Users Symposium, Texas A&M University, Houston, TX, 1989, pp. 9–15.
[6] N. Brunetière, B. Tournerie, J. Frêne, TEHD lubrication of mechanical face seals in stable tracking mode. Part 2: Parametric study, Journal of Tribology 125 (2003) 617–627.
[7] B. Nau, Research in mechanical seals, in: Mechanical Seal Practice for Improved Performance, IMechE, 1990, pp. 186–213.
[8] F. Tachibana, S. Fukui, H. Mitsumura, Heat transfer in an annulus with an inner rotating cylinder, Bulletin of JSME 3 (1963) 119–123.
[9] C. Gazley, Heat-transfer characteristics of the rotational and axial flow between concentric cylinders, Transactions of the ASME 80 (1958) 79–90.
[10] P.R.N. Childs, C.A. Long, A review of forced convective heat transfer in stationary and rotating annuli, Proceedings of the Institution of Mechanical Engineers, Part C: Journal of Mechanical Engineering Science 210 (1996) 123–134.
[11] K.M. Becker, Measurement of convective heat transfer from a horizontal cylinder rotating in a tank of water, International Journal of Heat and mass Transfer 6 (1963) 1053–1062.
[12] J.C. Doane, T.A. Myrum, J.E. Beard, An experimental-computational investigation of the heat transfer in mechanical face seals, International Journal of Heat and Mass Transfer (1991) 1027–1041.
[13] R.L. Phillips, L.E. Jacobs, P. Merati, Experimental determination of the thermal characteristics of a mechanical seal and its operating environment, Tribology Transactions 40 (1997) 559–568.
[14] P. Merati, N.A. Okita, R.L. Phillips, L.E. Jacobs, Experimental and computational investigations of flow and thermal behavior of a mechanical seal, Tribology Transactions 42 (1999) 731–738.
[15] A.O. Lebeck, M.E. Nygren, S.A. Shirazi, R. Soulizat, Fluid temperature and film coefficient prediction and measurement in mechanical face seals-experimental results, Tribology Transactions 41 (1998) 411–422 .
[16] S.A. Shirazi, R. Soulisa, A.O. Lebeck, M.A. Nygren, Fluid temperature and film coefficient prediction and measurement in mechanical face seals – numerical results, Tribology Transactions 41 (1998) 459–470.
[17] Z. Luan, M.M. Khonsari, Numerical simulations of the flow field around the rings of mechanical seals, Journal of Tribology 128 (2006) 559–565.
[18] J.M. Owen, R.H. Rogers, Flow and Heat Transfer in Rotating-Disc Systems – Volume 1 – Rotor Stator Systems, Research Studies Press LTD, Somerset, 1989.
[19] J. Daily, R. Nece, Chamber dimension effects on induced flow and frictional resistance of enclosed rotating disks, ASME Transactions, Journal of Basic Engineering 82 (1960) 217–232.
[20] H. Schlichting, Boundary Layer Theory, McGraw-Hill, New York, 1960.
[21] D. Dijkstra, G.J.F. van Heijst, Flow between two finite rotating disks enclosed by a cylinder, Journal of Fluid Mechanics 128 (1983) 123–154.
[22] J.M. Lopez, Flow between a stationary and a rotating disk shrouded by a co-rotating cylinder, Physics of Fluids 8 (1996) 2605–2613.
[23] R. Boutarfa, S. Harmand, Local convective heat transfer for laminar and turbulent flow in a rotor-stator system, Experiments in Fluids 38 (2005) 209–221.
[24] D. Reungoat, B. Tournerie, Temperature measurement by infrared thermography in a lubricated contact: Radiometric analysis, in: Proceedings of Quantitative Infrared Thermography QIRT94 (Eurotherm Seminar n^{o} 42), Elsevier, Paris, 1995.